Macromolecules
ARTICLE

Macromolecules **2010**, *43*, 615–624 **615**
DOI: 10.1021/ma902232g

Morphology and Mechanical Properties of Rubber Toughened Amorphous Polyamide/MMT Nanocomposites

Youngjae Yoo,[†] Lili Cui,[†] P. J. Yoon,[‡] and D. R. Paul*,[†]

[†]*Department of Chemical Engineering and Texas Material Institute, The University of Texas at Austin, Austin, Texas 78712 and* [‡]*Southern Clay Products, 1212 Church Street, Gonzales, Texas 78629*

Received October 7, 2009; Revised Manuscript Received December 7, 2009

ABSTRACT: The effects of addition of an organoclay on the morphology and the mechanical properties of blends of an amorphous polyamide (a-PA) and an elastomer (with and without grafted maleic anhydride) prepared via melt processing are reported. Transmission electron microscopy (TEM) and wide-angle X-ray scattering (WAXS) were employed to obtain a detailed quantitative analyses of the morphology of the elastomer particles for these nanocomposites containing 80 wt % a-PA and 20 wt % elastomer. Stress−strain diagrams and impact strength were measured as a function of organoclay content for blends containing maleated and unmaleated elastomer. It is clear that the addition of organoclay to blends can be an effective way for reducing elastomer particle size and enhancing stiffness when the elastomer is not maleated; however, for this system, toughness is not improved in spite of these morphological changes. Blends based on the maleated elastomer give a more beneficial balance of toughness versus stiffness.

Introduction

Toughening of semicrystalline polyamides like nylon-6 and -66 using maleated elastomers has been described in numerous reports.[1−8] A main focus has been on tailoring the morphology of the dispersed elastomer phase to achieve high levels of toughening by the *in situ* reaction between maleic anhydride grafted to the rubber and the polyamide amine end groups during melt compounding.[5,6,9−12] Also, it has been reported that the characteristics of the elastomer and the matrix polymer, the morphology of the dispersed phase, elastomer content, and processing conditions play an important role in determining the level of toughening of semicrystalline polyamides.[1,4−7,12,13] It is well-known that elastomer particle size is key to achieving supertoughness of polyamides; generally, there are optimum limits of particle size for toughening which vary with the polyamide type and molecular weight in addition to the elastomer type.[6,12] In contrast, there are very few reports on rubber toughening of amorphous polyamides;[10,11,14] however, our laboratory recently reported the toughening of an amorphous polyamide (Zytel 330 from DuPont, called a-PA here) using maleated elastomers.[10,11] The size of the elastomer particles in the blend was significantly decreased because of the reaction of the grafted maleic anhydride groups with the amine end groups of the polyamide to form graft copolymers that retard the coalescence of elastomer particles and enhance the interfacial adhesion between polyamide and elastomer. Generally, the mechanical properties of a polymer blend containing an elastomer depend critically on several aspects of the elastomer phase morphology such as particle size, uniformity of spatial distribution, elastomer phase volume, particle size distribution, etc.[15−19] Specifically, the elastomer particle size must be controlled within an optimal range in order to achieve supertoughness of polyamides. Details of the rubber toughening of nylon-6 and -66 with maleated rubber can be found in recent papers.[4,6,9−12]

*To whom all correspondence should be addressed: e-mail drp@che.utexas.edu, Tel +1-512-471-5392, Fax +1-512-471-0542.

Polymer nanocomposites containing an organoclay as a filler can lead to improved performance and opportunities for commercial applications.[20−24] Besides their reinforcing effect, it has been observed that organoclay particles can dramatically reduce the size of the dispersed phase in a polymer blend.[25−34] It is believed that high aspect ratio nanoparticles located between particles of a dispersed polymer phase sterically inhibit the coalescence of the polymer particles and, thereby, reduce their size as does the graft copolymer formed in reactive systems. Thus, it is logical to ask whether such nanoparticles might provide a route to improved toughness when grafting reactions are not possible; however, these nanoparticles do not necessarily lead to the increased interfacial adhesion that a grafting reaction would. Actually, the one property that almost always decreases relative to that of the matrix polymer upon addition of organoclay is toughness. Thus, the applications of nanocomposites can be limited by the reduction of toughness; therefore, rubber toughening of nanocomposites can be a potential route to a unique balance between toughness, strength, and other properties.[29,35,36] Recently, considerable efforts have been made to improve the toughness of nanocomposites by the addition of elastomer. Tjong et al.[37,38] reported that the SEBS-*g*-MA addition enhances the ductility of nanocomposites based on polyamide-6 and polypropylene at the expense of tensile strength and stiffness. González et al.[39] observed supertough behavior of 70/30 PA 6/SEBS-*g*-MA blends with 3 wt % organoclay content accompanied by a modulus increase of 44% with respect to the pure PA-6 matrix. Kusmono et al.[40] and Chow et al.[41] showed that the toughness and the stiffness in PA-6/polypropylene (PP) nanocomposites were improved by addition of SEBS-*g*-MA and maleic anhydride grafted ethylene−propylene rubber (EPR-*g*-MA), respectively. Lee et al.[29] observed the addition of organoclay to PP/EOR blends does result in significantly enhanced toughness especially at high elastomer contents. More recently, Martins et al.[42] reported a dramatic increase in the Izod impact strength and a considerable alteration of the shape the dispersed phase in nanocomposites from PP/EVA blends.

Published on Web 12/15/2009

Table 1. Materials Used in This Study

material (designation in this paper)	commercial designation	specifications	supplier
a-PA[a]	Zytel® 330	[COOH]/[NH2]=4.5[b] T_g=127 °C $\overline{M}_n$=14000[c] $\overline{M}_w$=50000[c]	Du Pont
EOR	Exact™ 8201	28 wt% Octene MFR: ~22 g/10 min density = 0.884 g/cc	ExxonMobil
EOR-*g*-MA	Exxelor™ MDEX 101-2	28 wt% Octene 1.6 wt% MA MFR: 19 g/10 min density = 0.8913 g/cc	ExxonMobil
$M_3(HT)_1$[d] Trimethyl hydrogenated-tallow ammonium montmorillonite	*Experimental*:	Organic loading = 95 mequiv/100 g clay Organic content = 29.6 wt % d_{001} spacing = 18.0 Å[e]	Southern Clay Products

[a] 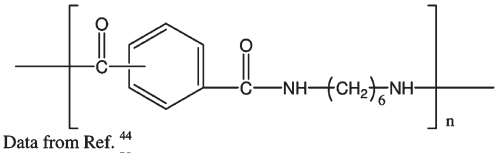

[b] Data from Ref. [44]
[c] Data from Ref. [75]
[d] The selected organoclay is designated as $M_3(HT)_1$ in this study, where M = methyl and HT = hydrogenated-tallow. Tallow is a natural product composed predominantly (63%) of saturated and unsaturated C_{18} chains. HT is the saturated form yet still contains a small fraction of double bonds.
[e] The basal spacing corresponds to the characteristic Bragg reflection peak d_{001} obtained from a powder WAXS scan of the organoclay.

Because of our prior experience with toughening a-PA with maleated ethylene−octene rubber, EOR-*g*-MA,[9−11] and with organoclay nanocomposites formed from a-PA,[43] this system was selected to explore the question of whether controlling the size of nonreactive elastomer particles, e.g., EOR, by adding an organoclay can be a strategy for toughening. A further objective of the present study was to explore the modulus versus toughness balance of amorphous polyamide (a-PA) nanocomposites toughened by the more conventional approach of adding EOR-*g*-MA.

Experimental Section

Materials. Table 1 summarizes the materials used in this study. The amorphous polyamide, a-PA, chosen for this study, Zytel 330, was supplied by DuPont. It has a glass transition temperature of 127 °C and a number-average molecular weight of 14 000. The majority of the chain ends of a-PA are [COOH] groups,[44] i.e., [COOH]/[NH_2] = 4.5 as shown in Table 1. Polyamides such as nylon-6 or nylon-66 typically have balanced [COOH] and [NH_2] groups, i.e., [COOH]/[NH_2] ≈ 1, unless the polyamide is made to be rich in one of the end-groups for some particular purpose.[10] The ethylene−1-octene copolymer, designated as EOR (Exact 8201), and a maleated version of this elastomer, designated as EOR-*g*-MA (Exxelor MDEX 101-2), were supplied by ExxonMobil. These have been used in prior work from our laboratory.[6,9−11] The organically modified clay, designated here as $M_3(HT)_1$, is an experimental product from Southern Clay Products formed by cation exchange reaction between sodium montmorillonite (Na^+ MMT) and a one-tailed quaternary ammonium surfactant, trimethyl hydrogenated-tallow ammonium chloride. Selected properties are also included in Table 1, and the choice of this organoclay is based on previous studies about the effect of organoclay structure on organoclay exfoliation in a-PA based nanocomposites.[43,45,46] These studies revealed that a-PA, like nylon-6, leads to better clay exfoliation with $M_3(HT)_1$ than with multiple-tailed organic modifiers.

Melt Processing. Prior to melt processing, a-PA was dried for a minimum of 24 h in a vacuum oven at 65 °C while the organoclay was used as-received. The a-PA/elastomer blends containing organoclay were formed via the following sequence of operations: first, melt compounding of the organoclay and a-PA to make a nanocomposite and, second, melt compounding of the nanocomposite with EOR or EOR-*g*-MA for toughening. Melt compounded composites were prepared using a Haake corotating, intermeshing twin-screw extruder (diameter = 30.5 mm, L/D = 10) operating at a barrel temperature of 240 °C, a feed rate of ~1 kg/h, and screw speed of 280 rpm. For comparison, a-PA/EOR or EOR-*g*-MA blends without the organoclay were also prepared and passed through the extruder twice so that they have the same thermal and shear history as nanocomposites prepared here. According to our prior studies,[45,47] the amount of MMT in each nanocomposite was confirmed by placing predried nanocomposites pellets in a furnace at 900 °C for 45 min and weighing the remaining MMT ash. Nanocomposite pellets were injection-molded to prepare standard 3.18 mm thick tensile (ASTM D638) and Izod bars (ASTM D256) using an Arburg All-rounder 305-210-700 injection molding machine using a barrel temperature of 240 °C, mold temperature of 80 °C, injection pressure of 70 bar, and a holding pressure of 35 bar. After molding, the samples were immediately sealed in a polyethylene bag and placed in a vacuum desiccator for a minimum of 24 h prior to testing. In this work, the a-PA/elastomer weight ratio was fixed at 80/20. A total elastomer phase concentration of 20 wt % has been used extensively in several prior works and reflects the range of commercial rubber-modified polyamides since it is known to provide a reasonable balance of impact properties versus stiffness.

Transmission Electron Microscopy. Samples for TEM analysis were taken from the core portion of an injection-molded bar. Ultrathin sections of ~50 nm thickness were cryogenically cut with a diamond knife at a temperature of −50 °C using an RMC PowerTome XL microtome. These sections were taken from the plane defined by the flow direction (FD) and the normal direction (ND) of the molded bar as explained elsewhere.[48,49] Sections were collected using 300-mesh grids and dried using filter paper and subsequently examined at an accelerating voltage of 120 kV using a JEOL 2010F TEM equipped with a field emission gun. Samples for observing elastomer particle size were chosen, and the polyamide phase was stained for an hour with a 2 wt % aqueous solution of phosphotungstic acid (PTA).

Particle Size Analyses. A quantitative analysis of elastomer particle size was performed from similar TEM micrographs

using the NIH ImageJ software as described previously.[10,11] At least four micrographs were used to analyze at least 800 elastomer particles from two different Izod bars, in order to adequately characterize the particle distribution. For nanocomposites with much larger elastomer particle sizes, at least 10 micrographs from two different Izod bars were used to obtain at least 100 rubber particles for analysis. Detailed discussions of the calculation of number- and weight-average elastomer particle sizes are available elsewhere.[10,11] Because of the nonspherical shape of the elastomer particles, no attempts were made to convert apparent particle diameters into the true dimensions.[35,50−54]

X-ray Analyses. Wide-angle X-ray scattering (WAXS) analyses were performed primarily in the reflection mode by a Scintag XDS 2000 diffractometer using Cu Kα radiation source (λ = 0.154 nm), set at a scan rate of 1.0°/min, a voltage = 45 kV, and current = 40 mA. The organoclay used in this work, $M_3(HT)_1$, was scanned in the form of powder while injection-molded samples of nanocomposites formed from them were also scanned such that the beam probed the skin of an Izod bar perpendicular to the FD. For certain samples, the skin of the bar was removed by an automated milling machine prior to the WAXS scans in order to obtain information about the morphology in the core of the bar as explained elsewhere.[43,55]

Mechanical Testing. Stress−strain analyses were performed at room temperature according to ASTM D638 using an Instron model 1137 testing machine upgraded for computerized data acquisition. Values of the tensile modulus were determined using an extensometer at a cross-head rate of 0.51 cm/min. For samples that yielded, complete stress−strain diagrams were measured at a cross-head rate of 5.1/min. Izod impact tests were conducted using a 6.8 J hammer and 3.5 m/s impact velocity at room temperature using a TMI Impact tester (model 43-02). Standard notches were made according to ASTM D256. Typically, data from at least five specimens were averaged to determine mechanical properties.

Morphology

TEM micrographs of nanocomposites formed from $M_3(HT)_1$ organoclay provide a direct visualization of the degree of organoclay dispersion in the elastomer or the a-PA/elastomer blend. Prior to discussing the morphology and properties of the blend nanocomposites, it is useful to explore the morphology of mixtures of the organoclay with the elastomers without a-PA. This reveals the compatibility between the elastomers and the organoclay used here and the propensity for the organoclay to enter elastomer domains when a-PA is present.

Nanocomposites Based on Elastomers (EOR or EOR-*g*-MA). Figure 1 shows TEM micrographs of the nanocomposites based on the two elastomers with 3 wt % organoclay. All views were taken from the plane defined by the flow direction (FD) and the normal direction (ND) of injection molded bars. Typical aggregates of MMT platelets are seen in Figure 1a for nanocomposite based on EOR only while relatively good dispersion of MMT platelets in EOR-*g*-MA is seen in Figure 1b. EOR has poor affinity for the organoclay having one alkyl tail, $M_3(HT)_1$, and therefore poor dispersion is achieved, as expected from previous investigations.[43,45,56] However, the anhydride group causes good affinity for the organoclay so that an partially exfoliated morphology was observed in EOR-*g*-MA as seen in Figure 1b.

Nanocomposites Based on a-PA/Elastomer. Figure 2 shows TEM micrographs for a-PA/elastomer nanocomposites with 5 wt % organoclay. In the case of EOR-containing nanocomposite, TEM micrographs like that in Figure 2a show that the organoclay is located in the a-PA phase or interface and not in the EOR phase. As we reported earlier,[43] a-PA has good affinity for $M_3(HT)_1$, and excellent

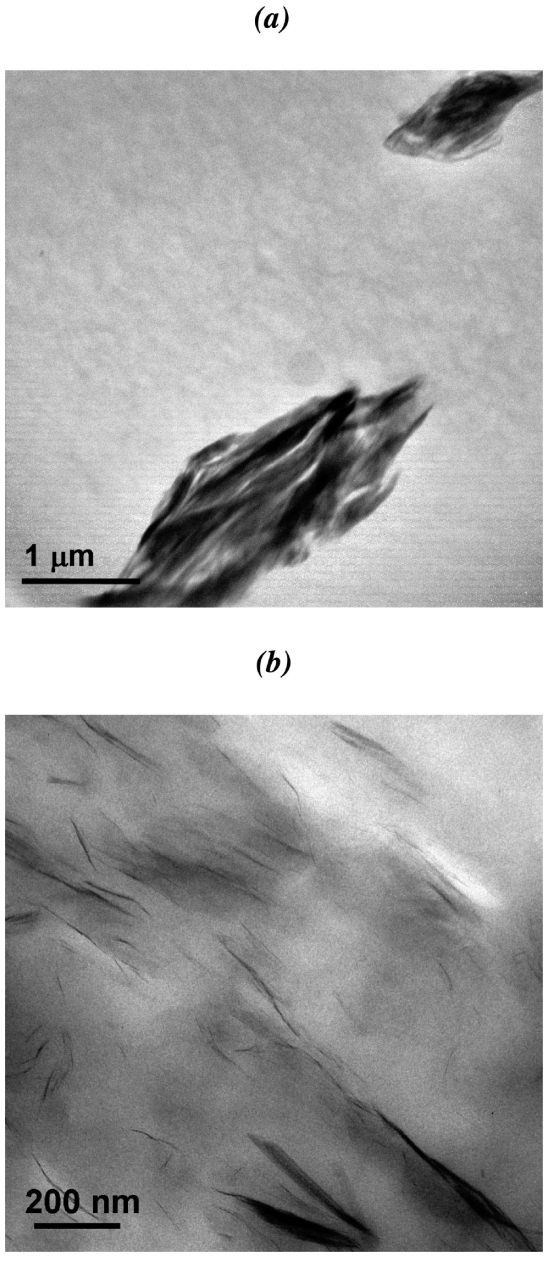

Figure 1. TEM micrographs of nanocomposites with 3 wt % organoclay based on (a) EOR and (b) EOR-*g*-MA.

exfoliation of the organoclay is observed. When blended with EOR, most clay particles are located in the a-PA phase, but some of the organoclay migrates into the a-PA/EOR interface and tends to envelop the EOR phase while maintaining the original ellipsoidal shape.[57] However, when blended with EOR-*g*-MA, quite different morphologies were observed. As mentioned above, EOR-*g*-MA has some affinity for the organoclay; as seen in Figure 2b, clay tactoids are seen in the a-PA phase, but some platelets are observed in the EOR-*g*-MA phase. However, because of the higher affinity of a-PA for the organoclay than EOR-*g*-MA, most of organoclay still locates in the a-PA phase. Figure 3 shows schematic representations of the morphological change in a-PA/elastomer nanocomposites that occur upon addition of organoclay. These schematics reflect the collective observations from many TEM micrographs.

WAXS is a commonly used technique for characterizing the exfoliation state of nanocomposites. Representative

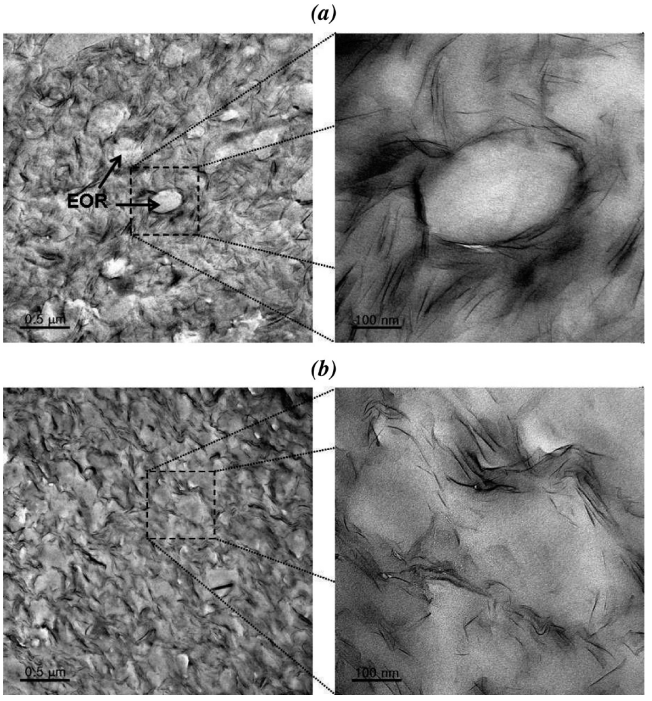

Figure 2. TEM micrographs of a-PA/elastomer (80/20) blend nanocomposites based on (a) EOR and (b) EOR-*g*-MA.

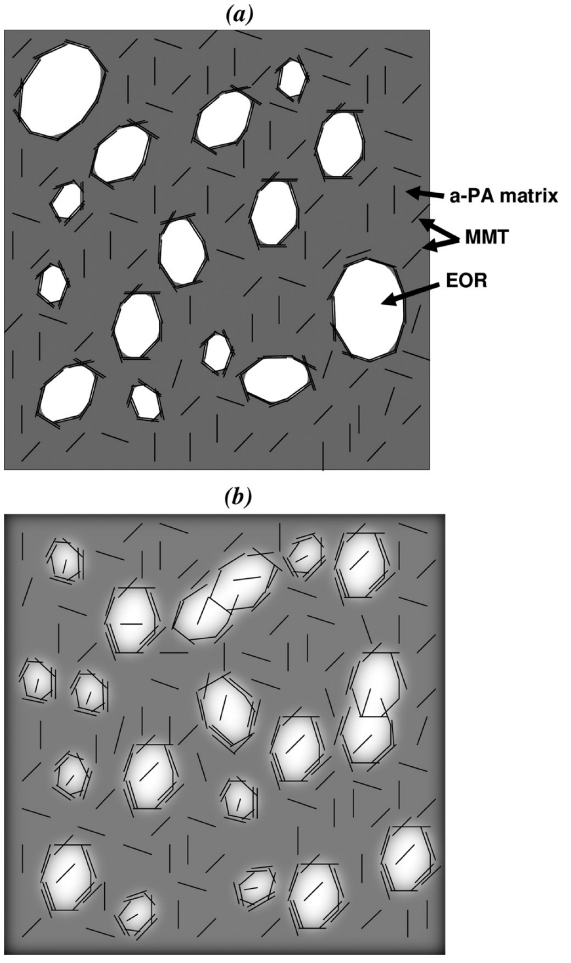

Figure 3. Schematic illustration of the morphological change in a-PA/elastomer blend nanocomposites based on (a) EOR and (b) EOR-*g*-MA.

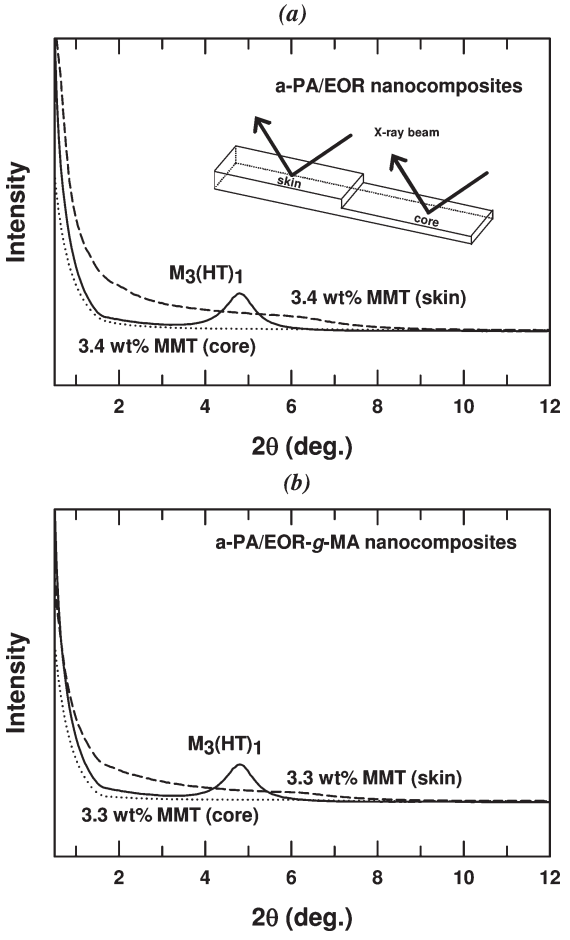

Figure 4. Skin and core effects on WAXS patterns of pristine organoclay and a-PA/elastomer bland (80/20) nanocomposites based on (a) EOR and (b) EOR-*g*-MA.

WAXS scans for the pristine organoclay and two corresponding nanocomposites are included and shown in Figure 4. To compare the structure between the skin and the core, some specimens were precision milled to half depth of the original bar thickness. Comparing the scans for the skin, nanocomposites from both EOR and EOR-*g*-MA have small diffraction peaks at approximately $2\theta = 6°-7°$. WAXS scans from the core of these nanocomposites, on the other hand, have no characteristic X-ray diffraction peaks. It is not reasonable to attribute these observations to differences in exfoliation levels from the skin to the core; a more likely explanation is that the clay particles are more oriented in the skin than the core as suggested by Lee et al.[29] Apparently, the lack of a diffraction peak from the tactoids in the core at this sensitivity reflects their disorder. Actually, the WAXS results provide only limited information about morphology while direct observation by TEM provides a more clear understanding of exfoliation levels. Of course, for TEM the observed area is rather small and a given image might not be representative of the nanocomposite as a whole. Thus, it is necessary to analyze multiple images to gain a full understanding of the morphology. Measurement of bulk properties such as mechanical, thermal, and dynamic mechanical properties complements TEM and WAXS analyses.[36,58]

Elastomer Morphology and Particle Analysis of Blend Nanocomposites. Figure 5 shows how the elastomer morphology of a-PA/elastomer blends described earlier depends on the addition of the organoclay. As can be seen in

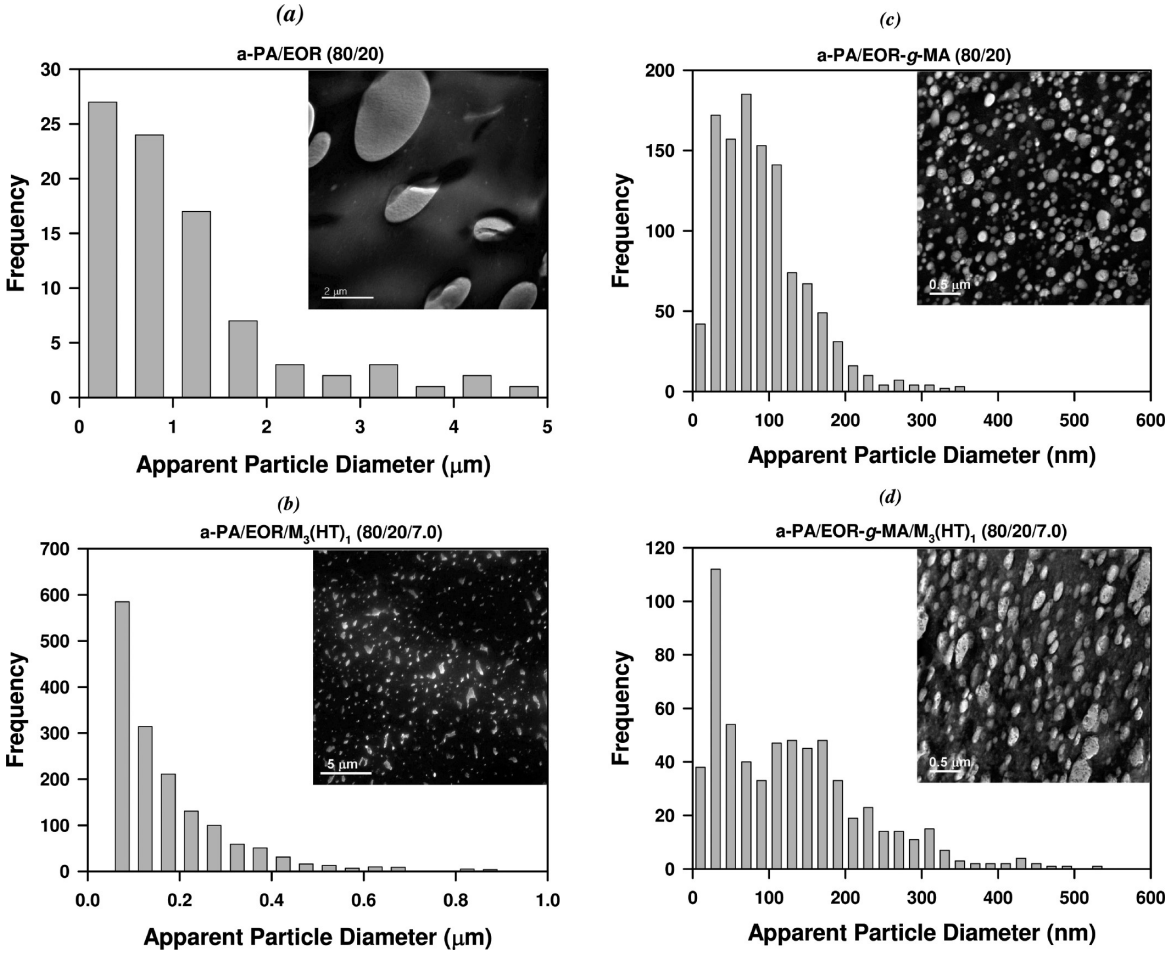

Figure 5. TEM micrographs and histograms of apparent elastomer particle size data obtained by analyzing TEM images of a-PA/elastomer blend (80/20) nanocomposites with/without maleation and with the following MMT contents: (a) EOR (0 wt % MMT), (b) EOR (7 wt % MMT), (c) EOR-*g*-MA (0 wt % MMT), and (d) EOR-*g*-MA (7 wt % MMT).

Figure 5a, without any organoclay a-PA/EOR blends have very large elastomer particles. For the a-PA/EOR nanocomposites with 7.0 wt % of the organoclay (Figure 5b), the elastomer particles are well dispersed in the a-PA matrix with a much smaller size and a more irregular shape compared to the a-PA/EOR blend. These apparent changes in the size and regularity of the elastomer phase may result from two competing effects during melt-processing; one is viscosity buildup of the matrix due to the presence of the organoclay while the other stems from a "barrier" effect of the clay particles on rubber particle coalescence.[26,28,29,32−34] It would appear that the inhibition of coalescence is the more effective mechanism for reducing elastomer particle size. On the other hand, blends of a-PA and EOR-*g*-MA with and without the organoclay show quite different elastomer morphology. Without the organoclay, the a-PA/EOR-*g*-MA blend in Figure 5c shows much smaller elastomer particles compared to the a-PA/EOR blend. Addition of organoclay to a-PA/EOR-*g*-MA blends does not cause a further reduction in the size of the elastomer particles; if anything, addition of organoclay causes a small increase in elastomer particle size. However, addition of organoclay does cause the elastomer particles to have a more extended ellipsoidal shape as shown in Figure 5d.

The qualitative assessments from TEM micrographs can be quantified by image analysis of the elastomer particles taken from these TEM micrographs using methods described elsewhere.[9−11,43,59,60] To determine the size of elastomer particles, the image analysis program used identifies each individual elastomer particle and evaluates its area, A. For simple comparison among nanocomposites, an apparent elastomer particle size, d, was calculated using the following relation:

$$d = \left(\frac{4A}{\pi}\right)^{1/2} \tag{1}$$

Representative histograms of apparent elastomer particle sizes defined by eq 1 for a-PA/(EOR or EOR-*g*-MA) nanocomposites containing 0 and 7 wt % organoclay are shown in Figure 5. Figure 6 shows the number-average apparent elastomer particle sizes, $\overline{d}_n$, and weight-average apparent particle sizes, $\overline{d}_w$, calculated from such histograms as a function of organoclay content. The number- and weight-average apparent elastomer particle sizes for a-PA/EOR nanocomposites decrease significantly with addition of organoclay content. The weight-average elastomer particle size in the a-PA/EOR blend without organoclay is 2.06 μm. The addition of 7.0 wt % of the organoclay decreases the weight-average elastomer particle size to 0.29 μm. However, EOR-*g*-MA containing nanocomposites have relatively similar elastomer particle sizes, 0.1−0.2 μm, over the entire range of organoclay contents.

For EOR-*g*-MA containing nanocomposites, the elastomer particles have a rather extended ellipsoidal shape as shown in Figure 5d. This feature can be quantified by introducing the concept of a "circularity ratio".[50−53]

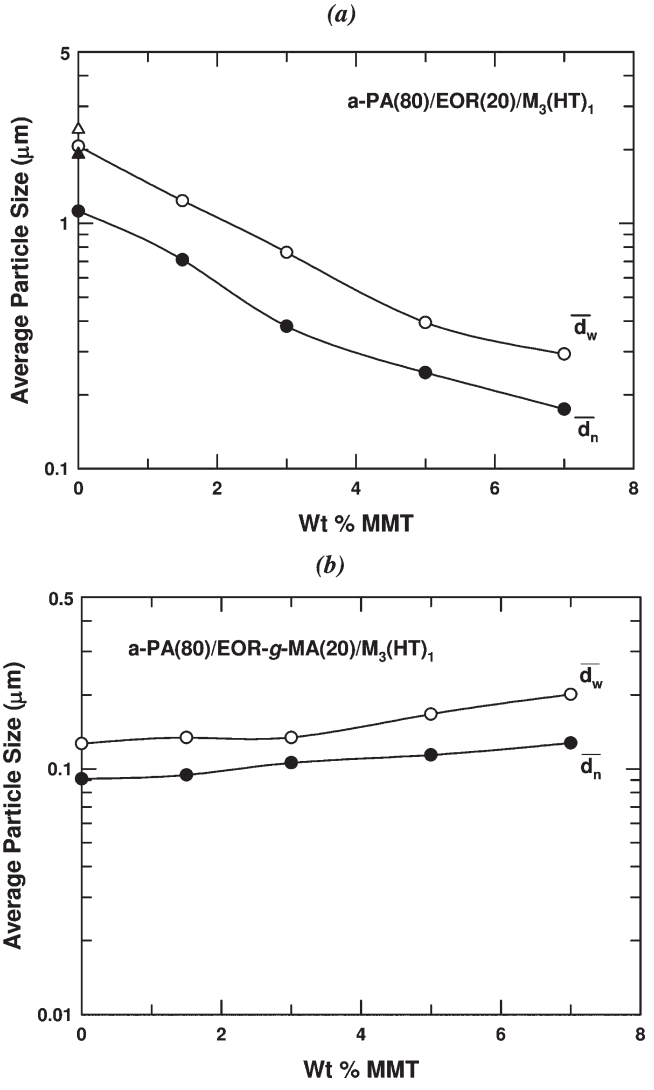

Figure 6. Effect of MMT levels on the number- and weight-average elastomer particle sizes of a-PA/elastomer blend (80/20) nanocomposites containing (a) EOR and (b) EOR-*g*-MA.

This is a dimensionless quantity defined as follows:

$$\text{circularity ratio} = C = 4\pi\frac{\text{area}}{(\text{perimeter})^2} \tag{2}$$

A circularity ratio of 1 means a true circular shape while $C = \pi/4$ corresponds to a square and $C = 0$ would describe an infinitely long and narrow shape. As shown in Figure 7, the circularity values for EOR-*g*-MA containing nanocomposites decrease with MMT concentration while those for EOR containing nanocomposites exhibit the opposite trend. The quantitative values of C agree with the shapes seen quantitatively in the TEM images.

Interfacial Tensions and Spreading Coefficients

Hobbs et al. showed how interfacial forces influence the morphology of multiphase polymer blends during melt processing.[61] They employed the concept of a spreading coefficient, λ_{ij}, defined according to Harkin's equation[62]

$$\lambda_{32} = \gamma_{21} - \gamma_{31} - \gamma_{23} \tag{3}$$

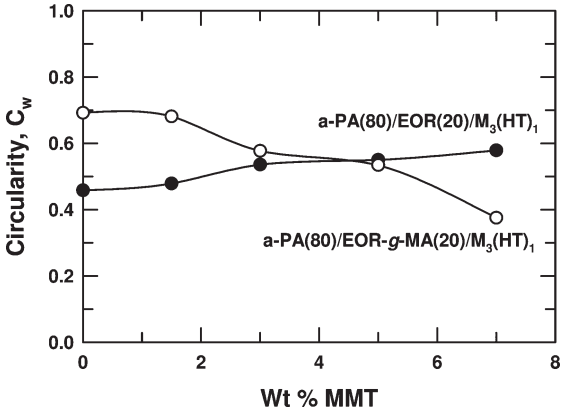

Figure 7. Effect of MMT levels on the circularity ratio of a-PA/elastomer blend (80/20) nanocomposites.

where γ_{21}, γ_{31}, and γ_{23} are the interfacial tensions for each component pair. The term λ_{32} indicates the spreading coefficient for the shell forming component 3 on the core forming component 2 in a matrix of component 1.[63−66] Essentially, if λ_{32} is positive, component 3 will have an interfacial driving force to spread over and encapsulate component 2. When both λ_{32} and λ_{23} are negative, components 2 and 3 will tend to disperse separately.[63−65] Virgilio et al.[63] recently emphasized that knowledge of all three spreading coefficients is necessary to properly predict the morphology. In the current system, γ_{12}, γ_{32}, and γ_{13} correspond to the interfacial tensions of a-PA/EOR, organoclay/EOR, and a-PA/organoclay (i.e., a-PA = 1, EOR = 2, and organoclay = 3), respectively.

The interfacial tensions γ_{12}, γ_{32}, and γ_{13} were estimated from the harmonic mean equation[67]

$$\gamma_{12} = \gamma_1 + \gamma_2 - 4\left[\frac{\gamma_1^{\mathrm{d}}\gamma_2^{\mathrm{d}}}{\gamma_1^{\mathrm{d}} + \gamma_2^{\mathrm{d}}} + \frac{\gamma_1^{\mathrm{p}}\gamma_2^{\mathrm{p}}}{\gamma_1^{\mathrm{p}} + \gamma_2^{\mathrm{p}}}\right] \tag{4}$$

where the superscripts d and p refer to the dispersive and polar contributions to the surface tension γ_i for component i, respectively. Equation 4 is meaningful only if the surface tensions are determined at the processing temperature. So, the values used in eq 4 should be extrapolated to the processing temperature on the basis of how surface tension varies with temperature ($d\gamma/dT$). For materials used here, experimentally measured values for γ and ($d\gamma/dT$) are available and were extracted directly from various references.[67−71] Estimates of the surface tensions at the processing temperature are listed in Table 2. As seen there, the spreading coefficient for organoclay on EOR in a-PA, λ_{32}, is +2.90 mN/m while for a-PA on EOR or EOR on a-PA, λ_{12} or λ_{21}, are −4.97 or −9.44 mN/m, respectively. The positive spreading coefficient for EOR and organoclay means that the organoclay is expected to envelop the EOR. On the other hand, the negative spreading coefficient for a-PA and EOR indicates the morphology in which a-PA and EOR phases are dispersed separately. The lowest value of the interfacial tension was observed for a-PA and organoclay, indicating the affinity of organoclay to a-PA rather than EOR. From this observation, it can be inferred that organoclay is more likely to be located in a-PA phase, and also organoclay will envelop the EOR as shown. In addition, the ratio $(\gamma_{13} - \gamma_{23})/\gamma_{12}$ can be a useful way to predict the equilibrium location of particles in a blend as shown by Cheng et al.[64] When this ratio has a value between −1 and +1, there will be a minimum in surface energy when the particle is located within the interface. Thus, unless other issues dominate, the particles can become trapped at the interface by surface forces much like a leaf at an air−water interface. As listed in Table 2, in this case, this ratio has a value of

Table 2. Calculation of Interfacial Tensions and Spreading Coefficients

phase	material	surface tension [mN/m] total γ	dispersive γ^d	polar γ^p	interfacial tension, γ_{ij} [mN/m]	$(\gamma_{13} - \gamma_{23})/\gamma_{12}$	spreading coefficient, λ_{ij} [mN/m]
1	amorphous polyamide[a]	32.2	18.2	14.0	$\gamma_{12} = 7.21$		$\lambda_{12} = -4.97$
2	EOR[b]	30.3	26.4	3.9	$\gamma_{23} = 3.27$	−0.31	$\lambda_{21} = -9.44$
3	organoclay[c]	33.4	22.9	10.5	$\gamma_{13} = 1.04$		$\lambda_{32} = 2.90$

[a] Data from ref 69. Values for polyamide assumed to be same as polyamide-66. The values at 240 °C were calculated on the basis of data on the variation of surface tensions with temperature ($-d\gamma/dT$). [b] Data from ref 70. Surface tension data of EOR was determined from contact angle measurement at ambient temperature. Nevertheless, by considering this data they could reach a better understanding. [c] Data from ref 68. Values for organoclay were calculated after heat treatment for 7 min at 220 °C followed by 7 min at 250 °C.

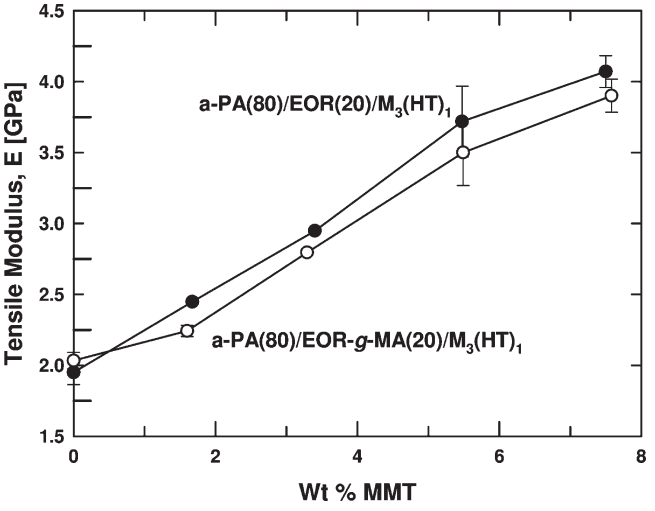

Figure 8. Effect of MMT content on tensile modulus of a-PA/elastomer blend (80/20) nanocomposites.

−0.31, which implies that at equilibrium the organoclay should be located at the interface; of course, some will remain in the a-PA phase. This is in good agreement with the TEM observations.

Mechanical Properties

Changes in mechanical properties reflect the extent of exfoliation of the organoclay in the a-PA/elastomer blends. Figure 8 shows the effect of organoclay concentration on the tensile modulus of nanocomposites prepared from a-PA containing 20 wt % EOR or EOR-*g*-MA. For both series of blends, there is a substantial increase in stiffness over the entire range of organoclay contents. Because most of the organoclay particles reside in the a-PA phase as demonstrated in Figure 2, the a-PA matrix is efficiently reinforced by the organoclay.

Figure 9 shows the stress−strain diagrams for the two blend series. The blends based on EOR-*g*-MA exhibit yielding followed by cold drawing. The yield stress increases while elongation at break decreases with addition of organoclay; both trends are as expected.[35] The blends based on EOR fracture prior to yielding. The break stress and strain both decrease as organoclay is added. These trends are consistent with observations for adding MMT to a brittle matrix.[72]

The notched Izod impact strength for a-PA/elastomer blends is shown in Figure 10. There is a very large difference in impact strength for the neat blends of a-PA/EOR versus a-PA/EOR-*g*-MA. The a-PA/EOR blend fails in a brittle manner in this test while the a-PA/EOR-*g*-MA blend is supertough. The high level of toughness for the latter can be attributed to the optimized particle sizes combined with good particle−matrix adhesion in the a-PA/EOR-*g*-MA blend owing to *in situ* reaction between maleic anhydride grafted to the elastomer and the polyamide amine end groups during melt compounding to form a graft copolymer;

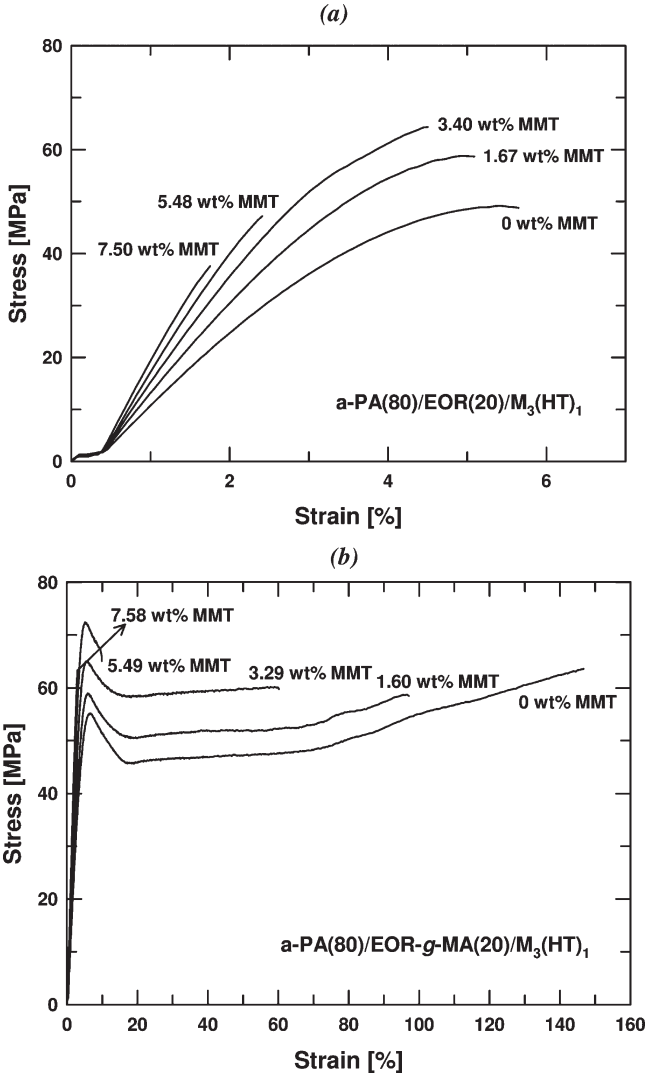

Figure 9. Stress−strain diagrams determined at 0.51 cm/mindrd for a-PA/elastomer blend (80/20) nanocomposites containing (a) EOR and (b) EOR-*g*-MA.

however, the elastomer particles in the a-PA/EOR blend are too large for efficient toughening. The addition of organoclay to the a-PA/EOR blend further decreases the impact strength in spite of the fact that the elastomer particle size is reduced to within the range where supertoughness could be expected. Similarly, adding organoclay to the a-PA/EOR-*g*-MA blend also dramatically decreases impact strength.

To explain the impact behavior for a-PA/elastomer blends based on EOR or EOR-*g*-MA in more detail, the effect of elastomer particle size on the Izod impact strength for these blends based on EOR or EOR-*g*-MA is shown in Figure 11.

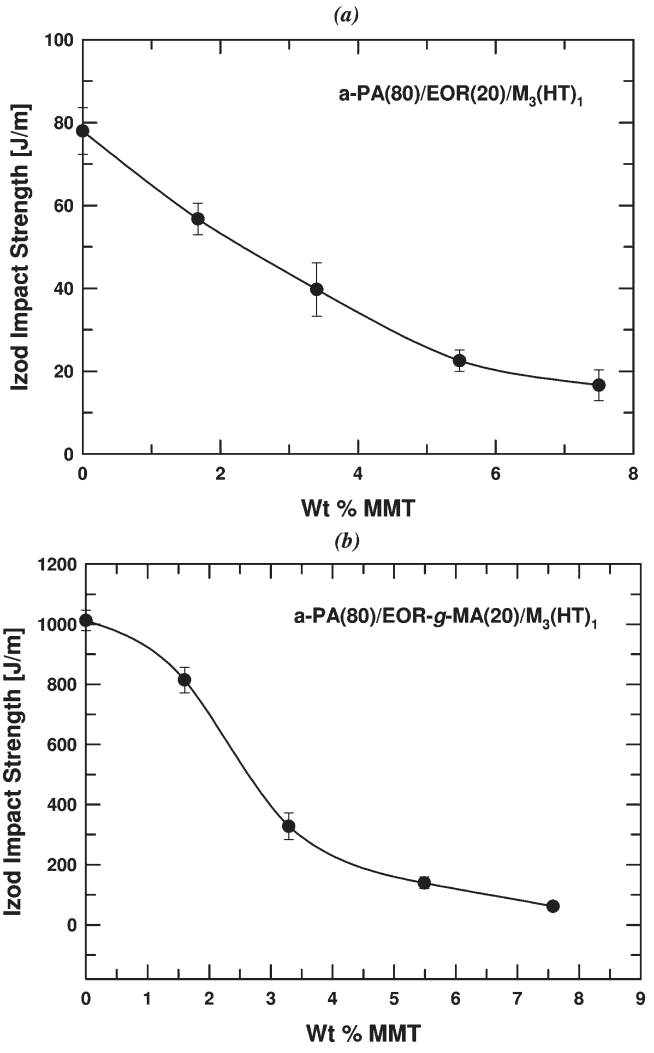

Figure 10. Effect of MMT content on the Izod impact strength of a-PA/elastomer blend (80/20) nanocomposites containing (a) EOR and (b) EOR-*g*-MA.

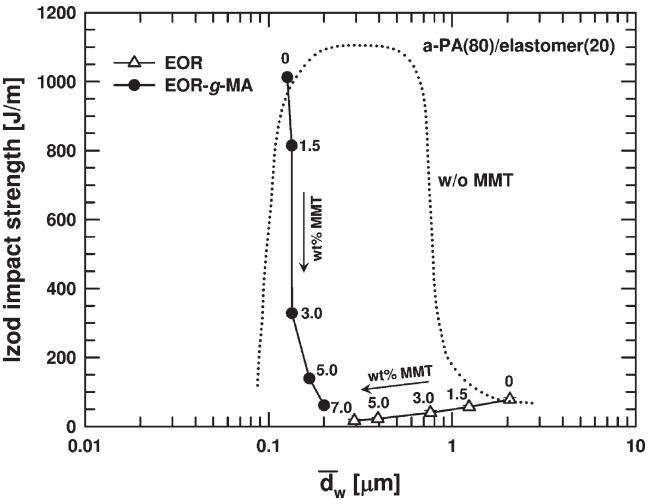

Figure 11. Effect of average elastomer particle sizes on the Izod impact strength of a-PA/elastomer blend (80/20) nanocomposites containing (a) EOR and (b) EOR-*g*-MA. Data for a-PA/EOR(-*g*-MA) blend without organoclay are from ref 9.

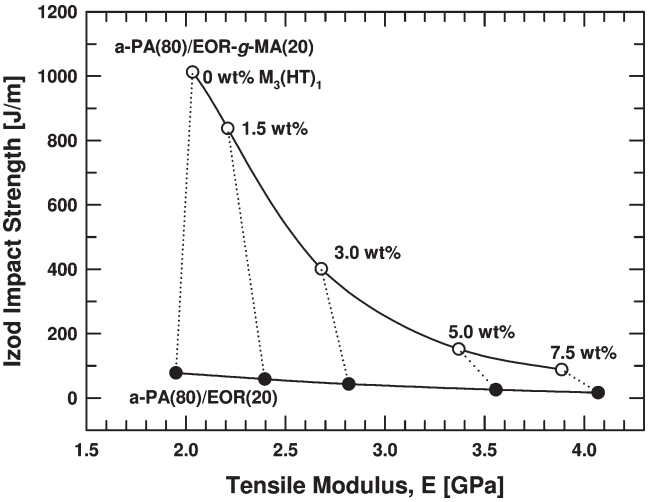

Figure 12. Relationship between impact strength and tensile modulus of a-PA/elastomer blend (80/20) nanocomposites.

For better understanding, the current data are compared with that observed earlier for a-PA/EOR-*g*-MA blends without organoclay shown as the dotted line in Figure 11.[9] For the latter blends, there is an optimum elastomer particle size, within the range of 0.15−0.8 μm, that leads to supertoughness. For the a-PA/EOR blend and its nanocomposite with 1.5 wt % MMT, the elastomer particle size is outside the optimum particle size, and a toughening effect is not expected. For a-PA/EOR nanocomposites with higher MMT content, the elastomer particle size moves within the range where significant toughening is expected (see dotted curve); however, these blends do not exhibit improved toughness. In fact, the toughness decreases as the elastomer particles become smaller by addition of clay.

For the a-PA/EOR-*g*-MA blend, the elastomer particles size is within the range where supertoughness can be expected as observed. Adding organoclay to this blend causes a slight increase in elastomer particle and shifts the size more toward the center of the optimum size range. The toughness of the blend decreases dramatically upon adding organoclays in spite of the elastomer particle size moving toward a more optimum value. To understand the effects shown here, it is important to remember that there are competing effects involved. The Izod value represents the area under a force−displacement curve.[35] While addition of clay increases the stiffness or the force levels in tensile tests as shown in Figure 8, it also reduces the extent of plastic deformation and can result in decreased impact strength. Appropriately dispersed maleated elastomer particles within a neat a-PA matrix increase toughness because under the triaxial stress state ahead the advancing crack tip the elastomer particles cavitate, if they are not too small, thereby allowing the a-PA matrix to shear yield and dissipate more energy.[35] Elastomer particles that are too large initiate crazes within the polyamide matrix and limits the toughening effect.[73] In fact, the toughening response is a very complicated process where yield strength, viscoelastic behavior, and other effects from the characteristics of the elastomer and the matrix polymer in addition to elastomer particle morphology all play some role.[9] From the results shown here, it appears that mechanical constraints imposed by the organoclay particles dominate over the effect the clay has on elastomer morphology.

To obtain an overview of the results and the trade-offs involved, the relationship between the Izod impact strength and tensile modulus for these blend nanocomposites is shown in Figure 12. For both a-PA/EOR and a-PA/EOR-*g*-MA blend nanocomposites, there is a trade-off relationship between the Izod impact strength and tensile modulus with addition of clay as observed in most nanocomposites systems.[35,43,46,74]

Conclusions

Blends of a-PA and unmaleated elastomer containing various levels of organoclay were prepared to explore the possibility of enhancing toughness by tailoring the elastomer particle size via the effect the organoclay on dispersed phase particle coalescence. Analyses of the morphology of a-PA/EOR nanocomposites show that most of the organoclay is well exfoliated in the a-PA phase, but some of the organoclay migrates to the interface and tends to envelop the EOR phase. The average elastomer particle sizes in a-PA/EOR blends decrease significantly with addition of organoclay. It seems that addition of organoclay to such blends can be an effective way for tailoring elastomer particle size and stiffness enhancement; however, for the present system, toughness is not improved by these changes in morphology. However, addition of organoclay to polypropylene/EOR blends does result in significantly enhanced toughness, especially at high elastomer contents. The reasons for these differences between the two systems are not yet clear but are being explored.

On the other hand, where EOR-*g*-MA is used instead, organoclay is still observed in the a-PA phase, but a few platelets are observed in the elastomer phase. The elastomer particle sizes in a-PA/EOR-*g*-MA blends are already very small owing to the reactive compatibilization that occurs; addition of organoclay slightly increases the size of the elastomer particles. The blends without organoclay are supertough owing to the optimized elastomer particle size. Addition of organoclay to such blends decreases the toughness; however, this system has a better balance of toughness versus stiffness than the one where the elastomer is unmaleated.

Acknowledgment. This work was supported in part by a grant from General Motors Global Research and Development; the authors thank William R. Rodgers for his continued interest. The authors sincerely thank D. L. Hunter of Southern Clay Products, Inc., for providing organoclay materials and many helpful discussions and Mr. Tony Gonzalez for his help with WAXS analyses.

References and Notes

(1) Borggreve, R. J. M.; Gaymans, R. J.; Schuijer, J.; Housz, J. F. I. *Polymer* **1987**, *28* (9), 1489–1496.
(2) Bucknall, C. B.; Heather, P. S.; Lazzeri, A. *J. Mater. Sci. Lett.* **1989**, *24* (6), 2255–2261.
(3) Corté, L.; Leibler, L. *Polymer* **2005**, *46* (17), 6360–6368.
(4) Dijkstra, K.; Wal, A. V. D.; Gaymans, R. J. *J. Mater. Sci.* **1994**, *29* (13), 3489–3496.
(5) Majumdar, B.; Paul, D. R.; Oshinski, A. J. *Polymer* **1997**, *38* (8), 1787–1808.
(6) Oshinski, A. J.; Keskkula, H.; Paul, D. R. *Polymer* **1992**, *33* (2), 268–283.
(7) Wu, S. *J. Appl. Polym. Sci.* **1988**, *35* (2), 549–561.
(8) Xanthos, M. *Polym. Eng. Sci.* **1988**, *28* (21), 1392–1400.
(9) Huang, J. J.; Keskkula, H.; Paul, D. R. *Polymer* **2006**, *47* (2), 639–651.
(10) Huang, J. J.; Keskkula, H.; Paul, D. R. *Polymer* **2006**, *47* (2), 624–638.
(11) Huang, J. J.; Keskkula, H.; Paul, D. R. *Polymer* **2004**, *45* (12), 4203–4215.
(12) Oshinski, A. J.; Keskkula, H.; Paul, D. R. *Polymer* **1996**, *37* (22), 4909–4918.
(13) Okada, O.; Keskkula, H.; Paul, D. R. *Polymer* **2000**, *41* (22), 8061–8074.
(14) Nielinger, W.; Brassat, B.; Neuray, D. *Angew. Makromol. Chem.* **1981**, *98* (1), 225–236.
(15) Bucknall, C. B. *Toughened Plastics*; Applied Science Publishers: London, 1977.
(16) Bucknall, C. B.; Davies, P.; Partridge, I. K. *J. Mater. Sci.* **1987**, *22* (4), 1341–1346.
(17) Fowler, M. E.; Keskkula, H.; Paul, D. R. *Polymer* **1987**, *28* (10), 1703–1711.
(18) Hobbs, S. Y. *Plastic Polymer Science and Technology*; Wiley-Interscience: New York, 1982.
(19) Keskkula, H.; Paul, D. R.; McCreedy, K. M.; Henton, D. E. *Polymer* **1987**, *28* (12), 2063–2069.
(20) Krishnamoorti, R.; Vaia, R. A. *J. Polym. Sci., Part B: Polym. Phys.* **2007**, *45* (24), 3252–3256.
(21) Usuki, A.; Kojima, Y.; Kawasumi, M.; Okada, A.; Fukushima, Y.; Kurauchi, T.; Kamigaito, O. *J. Mater. Res.* **1993**, *8* (5), 1185–1189.
(22) Usuki, A.; Kojima, Y.; Kawasumi, M.; Okada, A.; Fukushima, Y.; Kurauchi, T.; Kamigaito, O. *J. Mater. Res.* **1993**, *8* (5), 1179–1184.
(23) Vaia, R. A.; Giannelis, E. P. *MRS Bull.* **2001**, May, 394−401.
(24) Yoo, Y.; Kim, S.-S.; Won, J. C.; Choi, K.-Y.; Lee, J. H. *Polym. Bull.* **2004**, *52* (5), 373–380.
(25) Gahleitner, M.; Kretzschmar, B.; Vliet, G. V.; Devaux, J.; Pospiech, D.; Bernreitner, K.; Ingolic, E. *Rheol. Acta* **2006**, *45* (4), 322–330.
(26) Gelfer, M. Y.; Song, H. H.; Liu, L.; Hsiao, B. S.; Chu, B.; Rafailovich, M.; Si, M.; Zaitsev, V. *J. Polym. Sci., Part B: Polym. Phys.* **2003**, *41* (1), 44–54.
(27) Gersappe, D. *Phys. Rev. Lett.* **2002**, *89* (5), 058301-1–058301-4.
(28) Khatua, B. B.; Lee, D. J.; Kim, H. Y.; Kim, J. K. *Macromolecules* **2004**, *37* (7), 2454–2459.
(29) Lee, H.-S.; Fasulo, P. D.; Rodgers, W. R.; Paul, D. R. *Polymer* **2005**, *46* (25), 11673–11689.
(30) Si, M.; Araki, T.; Ade, H.; Kilcoyne, A. L. D.; Fisher, R.; Sokolov, J. C.; Rafailovich, M. H. *Macromolecules* **2006**, *39* (14), 4793–4801.
(31) Vo, L. T.; Giannelis, E. P. *Macromolecules* **2007**, *40* (23), 8271–8276.
(32) Voulgaris, D.; Petridis, D. *Polymer* **2002**, *43* (8), 2213–2218.
(33) Wang, Y.; Zhang, Q.; Fu, Q. *Macromol. Rapid Commun.* **2003**, *24* (3), 231–235.
(34) Yoo, Y.; Park, C.; Lee, S.-G.; Choi, K.-Y.; Kim, D. S.; Lee, J. H. *Macromol. Chem. Phys.* **2005**, *206* (8), 878–884.
(35) Ahn, Y.-C.; Paul, D. R. *Polymer* **2006**, *47* (8), 2830–2838.
(36) Kim, D. H.; Fasulo, P. D.; Rodgers, W. R.; Paul, D. R. *Polymer* **2007**, *48* (20), 5960–5978.
(37) Tjong, S. C.; Bao, S. P. *J. Polym. Sci., Part B: Polym. Phys.* **2005**, *43* (5), 585.
(38) Tjong, S. C.; Bao, S. P.; Liang, G. D. *J. Polym. Sci., Part B: Polym. Phys.* **2005**, *43* (21), 3112–3126.
(39) González, I.; Eguiazábal, J. I.; Nazábal, J. *Eur. Polym. J.* **2006**, *42* (11), 2905–2913.
(40) Kusmono; Ishak, Z. A. M.; Chow, W. S.; Takeichi, T.; Rochmadi. *Composites, Part A* **2008**, *39* (12), 1802–1814.
(41) Chow, W. S.; Bakar, A. A.; Ishak, Z. A. M.; Karger-Kocsis, J.; Ishiaku, U. S. *Eur. Polym. J.* **2005**, *41* (4), 687–696.
(42) Martins, C. G.; Larocca, N. M.; Paul, D. R.; Pessan, L. A. *Polymer* **2009**, *50* (7), 1743–1754.
(43) Yoo, Y.; Paul, D. R. *Polymer* **2008**, *49*, 3795–3804.
(44) Xanthos, M.; Parmer, J. F.; Forest, M. L. L.; Smith, G. R. *J. Appl. Polym. Sci.* **1996**, *62* (8), 1167–1177.
(45) Fornes, T. D.; Hunter, D. L.; Paul, D. R. *Macromolecules* **2004**, *37* (5), 1793–1798.
(46) Fornes, T. D.; Yoon, P. J.; Hunter, D. L.; Keskkula, H.; Paul, D. R. *Polymer* **2002**, *43* (22), 5915–5933.
(47) Shah, R. K.; Paul, D. R. *Polymer* **2004**, *45*, 2991–3000.
(48) Fornes, T. D.; Paul, D. R. *Macromolecules* **2004**, *37* (20), 7698–7709.
(49) Yoon, P. J.; Fornes, T. D.; Paul, D. R. *Polymer* **2002**, *43* (25), 6727–6741.
(50) Allen, T. *Particle Size Measurement*; Chapman & Hall: London, 1997.
(51) Barreiros, F. M.; Ferreira, P. J.; Figueiredo, M. M. *Part. Part. Syst. Charact.* **1996**, *13* (6), 368–373.
(52) Carter, R. M.; Yan, Y. *J. Phys.: Conf. Ser.* **2005**, *15*, 177–182.
(53) Irani, R. R.; Callis, C. F. *Particle Size: Measurement, Interpretation, and Application*; Wiley: New York, 1963.
(54) Mason, C. W. *Title Handbook of Chemical Microscopy*; Wiley: New York, 1982.
(55) Stretz, H. A.; Paul, D. R. *Polymer* **2006**, *47* (24), 8123–8136.
(56) Hotta, S.; Paul, D. R. *Polymer* **2004**, *45* (22), 7639–7654.
(57) Hong, J. S.; Namkung, H.; Ahn, K. H.; Lee, S. J.; Kim, C. *Polymer* **2006**, *47* (11), 3967–3975.
(58) Kim, D. H.; Fasulo, P. D.; Rodgers, W. R.; Paul, D. R. *Polymer* **2007**, *48* (18), 5308–5323.
(59) Cui, L.; Ma, X.; Paul, D. R. *Polymer* **2007**, *48* (21), 6325–6339.
(60) Cui, L.; Troeltzsch, C.; Yoon, P. J.; Paul, D. R. *Macromolecules* **2009**, *42* (7), 2599–2608.

(61) Hobbs, S. Y.; Dekkers, M. E. J.; Watkins, V. H. *Polymer* **1988**, *29* (9), 1598–1602.
(62) Harkins, W. D. *The Physical Chemistry of Surface Films*; Reinhold: New York, 1952; p 23.
(63) Virgilio, N.; Marc-Aurele, C.; Favis, B. D. *Macromolecules* **2009**, *42* (9), 3405–3416.
(64) Cheng, T. W.; Keskkula, H.; Paul, D. R. *Polymer* **1992**, *33* (8), 1606–1619.
(65) Liu, H.; Xie, T.; Zhang, Y.; Ou, Y.; Yang, G. *J. Polym. Sci., Part B: Polym. Phys.* **2006**, *44* (7), 1050–1061.
(66) Luzinov, I.; Xi, K.; Pagnoulle, C.; Huynh-Ba, G.; Jérôme, R. *Polymer* **1999**, *40* (10), 2511–2520.
(67) Wu, S. *Polymer Interface and Adhesion*; Marcel Dekker: New York, 1982.
(68) Dharaiya, D.; Jana, S. C. *Polymer* **2005**, *46* (23), 10139–10147.
(69) Owens, D. K.; Wendt, R. C. *J. Appl. Polym. Sci.* **1969**, *13* (8), 1741–1747.
(70) Premphet, K.; Horanont, P. *Polymer* **2000**, *41* (26), 9283–9290.
(71) Wu, S.-H.; Wang, F.-Y.; Ma, C.-C. M.; Chang, W.-C.; Kuo, C.-T.; Kuan, H.-C.; Chen, W.-J. *Mater. Lett.* **2001**, *49* (6), 327–333.
(72) Stretz, H. A.; Paul, D. R.; Li, R.; Keskkula, H.; Cassidy, P. E. *Polymer* **2005**, *46* (8), 2621–2637.
(73) Bucknall, C. B.; Paul, D. R. *Polymer* **2009**, *50* (23), 5539–5548.
(74) Yoon, P. J.; Hunter, D. L.; Paul, D. R. *Polymer* **2003**, *44* (18), 5323–5339.
(75) Ellis, T. S. *Macromolecules* **1991**, *24* (13), 3845–3852.